

Pointy ice-drops: How water freezes into a singular shape

Jacco H. Snoeijer and Philippe Brunet

Citation: *Am. J. Phys.* **80**, 764 (2012); doi: 10.1119/1.4726201

View online: <http://dx.doi.org/10.1119/1.4726201>

View Table of Contents: <http://ajp.aapt.org/resource/1/AJPIAS/v80/i9>

Published by the [American Association of Physics Teachers](#)

Related Articles

The quadratically damped oscillator: A case study of a non-linear equation of motion
[Am. J. Phys.](#) **80**, 816 (2012)

Why no shear in “Div, grad, curl, and all that”?
[Am. J. Phys.](#) **80**, 519 (2012)

Jacobi elliptic functions and the complete solution to the bead on the hoop problem
[Am. J. Phys.](#) **80**, 506 (2012)

Embeddings and time evolution of the Schwarzschild wormhole
[Am. J. Phys.](#) **80**, 203 (2012)

The Shape of Inner Space: String Theory and the Geometry of the Universe’s Dimensions
[Am. J. Phys.](#) **79**, 559 (2011)

Additional information on Am. J. Phys.

Journal Homepage: <http://ajp.aapt.org/>

Journal Information: http://ajp.aapt.org/about/about_the_journal

Top downloads: http://ajp.aapt.org/most_downloaded

Information for Authors: <http://ajp.dickinson.edu/Contributors/contGenInfo.html>

ADVERTISEMENT



Pointy ice-drops: How water freezes into a singular shape

Jacco H. Snoeijer

Physics of Fluids Group and J. M. Burgers Centre for Fluid Dynamics, University of Twente, P.O. Box 217, 7500 AE Enschede, The Netherlands

Philippe Brunet

Laboratoire Matière et Systèmes Complexes UMR CNRS 7057, Batiment Condorcet, 10 rue Alice Domont et Léonie Duquet 75205 Paris cedex 13, France

(Received 15 April 2011; accepted 22 May 2012)

A water drop that is gently deposited on a very cold surface freezes into a pointy ice-drop with a very sharp tip. The formation of this singular shape originates from the reduction of mass density during the freezing process and can be explained using a simplified model for which the universal structure of the singularity is revealed in full detail. The combination of a relatively simple, static experiment, and the accessible asymptotic analysis makes this system an ideal introduction to the topic of singularities. © 2012 American Association of Physics Teachers.

[<http://dx.doi.org/10.1119/1.4726201>]

I. INTRODUCTION

One of the most fascinating features encountered in fluid mechanics is the ability to create singular structures in space and time.^{1–8} These singularities are the consequence of flows that self-focus into a specific location and/or a given moment of time. Perhaps the best known singularity is encountered during drop formation, where a liquid thread pinches off under the action of surface tension.¹ Other examples are found in dewetting flows,^{2,3,7} during the penetration of one fluid into another,^{4,5,8} or in the formation of Taylor-cones in electrified fluids.⁶ These situations typically involve the formation of a cusp on the interface between two fluid phases.

Interestingly, it is known that surface tension tends to oppose the formation of these cusps. Indeed, the macroscopic action of surface tension is to generate a pressure difference across the interface proportional to the local curvature of the interface, which we could summarize by the motto: surface tension does not like sharp points. Thus, it is clear that any of the pointy structures described in Refs. 1–8 require complex and highly energetic processes. In fact, the cusp tip has a high, but finite, curvature. The driving force responsible for the singularity is balanced by surface tension on a scale that is much smaller than the scale of the flow. The consequence of this complex and dynamical equilibrium is that these singularities are challenging to access experimentally and often require high-speed and/or high-resolution cameras.

The freezing of water drops, on the other hand, provides a surprisingly simple example of the formation of a cusped singularity that is easy to generate and observe.^{9,10} Just place a drop of water onto a plate with a temperature far below the freezing point and wait. Starting from the bottom of the drop, the liquid will quickly freeze. Just before the freezing front reaches the top of the drop, the interface changes from a spherical to a pointy top that is reminiscent of the onion domes that appear on orthodox churches or minarets. As shown in Fig. 1, these pointy ice-drops offer a static, frozen cusp that can be analyzed in detail.

From a practical perspective, these freezing drops are encountered in icing of water during flights¹¹ where frozen accreted water can cause damage to the cabin of aircrafts. More generally, the formation of frost and how it can be delayed is of fundamental interest to material scientists.^{12,13}

At much smaller scales, similar pointy structures at the tip of crystal spikes form during solidification processes on water, silicon, or germanium.¹⁴ These pointy structures only seem to appear for liquids that expand upon freezing.

The formation of the cusp can be described by an elegant geometric model originally proposed by Sanzet *al.*¹⁰ and later generalized by Anderson *et al.*⁹ The key ingredient to produce the cusp is that the density of the solid phase is lower than that of the liquid phase. Mathematically, the model relies mainly on geometry and is therefore accessible to students at the undergraduate level. Importantly, no background knowledge of fluid mechanics is necessary. In addition, the model allows for an asymptotic analysis that gives students a taste of the methods used to analyze singularities. This combination of a relatively simple, static experiment, and an accessible asymptotic analysis makes these ice-drops a unique introduction to the topic of singularities.

The rest of this paper is organized as follows. In Sec. II, we present the experimental setup. Section III introduces the mathematical model used to understand the formation of the cusps and discusses how the model can be solved numerically. In Sec. IV, we present a detailed asymptotic analysis to reveal the fine structure of the singularity. Finally, a concluding discussion is given in Sec. V.

II. EXPERIMENTAL SETUP

The formation of singular ice-drops can be studied with the relatively simple experimental setup shown in Fig. 2(a). A smooth plate with good thermal conductivity (copper, steel, or silicon) is cooled to a temperature between 200 K and 250 K. This is achieved by placing the plate in a polystyrene box filled with liquid nitrogen. The temperature of the plate is measured with a thermocouple in contact with the surface. Once the plate has cooled significantly, the temperature will remain stable for the duration of the experiment (typically a few minutes). To allow for an unobstructed view of the drop profile, the top surface of the plate must be higher than the edges of the polystyrene box.

The experiment begins by gently depositing a drop of water on the plate using a syringe. Typical drop volumes range from 10 to 20 μl , which corresponds to millimeter-sized drops. For these volumes, the drops take the shape of a nearly perfect spherical cap, suggesting that gravity can be



Fig. 1. Pointy ice drops frozen on a cold plate. The ice drops are formed from millimeter sized water drops that were gently deposited on the surface. The singular shape at the top of the drop appears spontaneously towards the end of the freezing process. Note that tiny ice crystals are formed on the sharp tips of the drops, which is due to the freezing of the surrounding vapor.

neglected. The dimensionless parameter that quantifies the importance of gravity compared to surface tension is the Bond number, defined as

$$\text{Bo} = \frac{\rho g \mathcal{R}^2}{\gamma}, \quad (1)$$

where \mathcal{R} is the radius of a perfect sphere of the same volume, ρ and γ are the liquid density and surface tension, respectively, and g is the gravitational field strength. For the volumes cited above, the Bond number ranges from 0.25 to 0.4, confirming that surface tension forces dominate over gravity.

The timescale for droplet freezing is typically around 10–30 s; thus, no high-speed imaging techniques are required to follow the process. In fact, one can simply take pictures with a still camera after the entire drop is frozen. To obtain an accurate drop profile, the pictures must be taken at a very small angle with respect to the horizontal [see Fig. 2(b)].

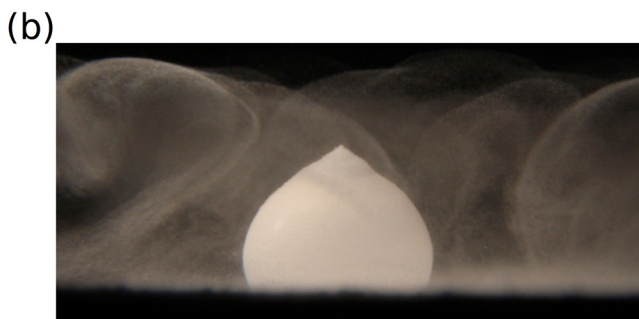
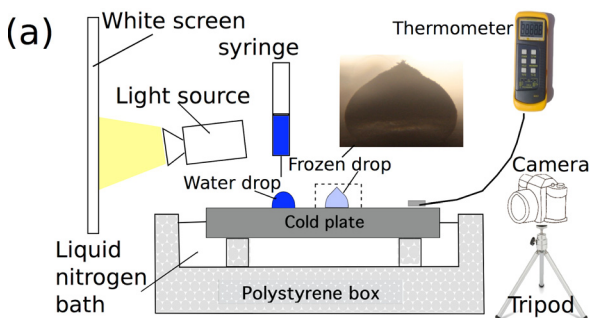


Fig. 2. (a) Schematic representation of the experimental setup. (b) Typical experimental photograph from a frozen ice-drop. Note the mist of frozen water vapor that deposits ice crystals on the drop.

Installing the camera on a tripod makes it easier to adjust shutter speeds and aperture settings to obtain a good contrast image. Special care must be taken to avoid the mist produced by the cooling of water vapor in the vicinity of the plate. This mist diffuses the light and can make it difficult to obtain clear images. We have obtained high contrast images by either backlighting a white screen behind the drops or shining a bright light directly on the front of the drops.

A qualitative description of the freezing process is as follows. Due to the very cold temperature of the substrate, the bottom of the drop freezes first. This means the solidification of the water occurs through a sharp ice/water front that moves upwards over time. The freezing process is completed once the front has invaded the entire liquid phase. It is only during the last few moments of freezing that the shape of the droplet top turns from round to pointy.¹⁹

After the water is transformed into ice, the frozen droplet is progressively covered with tiny ice crystals that self assemble on its top. Thus, the initially smooth solid/vapor interface becomes increasingly rough over time. This solidification of water vapor on the frozen droplet is most efficient at the sharp tip, as is visible in Fig. 1. We will discuss this phenomenon in detail in Sec. V.

III. MODEL FORMULATION

A. Geometric model

To make a quantitative model for the ice-drops, we need to know the exact shape of the ice/water front as it propagates during the freezing process. This propagation is a complicated process that depends on the details of heat transfer inside the drop.¹⁶ In addition, the dynamics near the three-phase contact line, where the liquid, solid, and vapor phases meet, is not fully understood and is the subject of current research.^{9,15} Therefore, a fully quantitative model that is able to accurately predict the shape of these ice drops is beyond the scope of this paper.

Fortunately, it is possible to illustrate the physics underlying the pointy drops with a simplified version of the models proposed in the literature.^{9,10} The basic idea is sketched in Fig. 3. First, it is assumed that the ice/water interface remains horizontal during the solidification process. A second assumption is that freezing along the surface occurs in the direction along the water/vapor interface, characterized by the contact angle θ [Fig. 3(a)]. In other words, the slope of the ice layer is identical to the slope of the liquid spherical cap at the contact line. As we show below, this framework indeed reproduces singular, pointy ice-drops for liquids that have a lower density

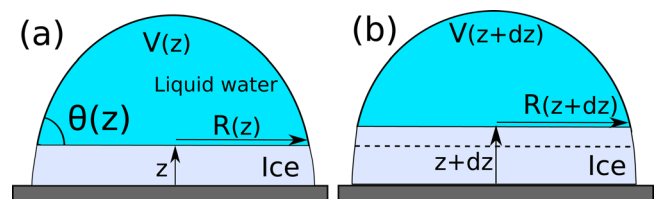


Fig. 3. Geometric model for the solidification of the water drop. (a) The water/ice interface is assumed to be perfectly horizontal, and the shape of the unfrozen water is assumed to be that of a spherical cap. The geometry is entirely determined by the base radius of the unfrozen liquid R , the water volume V , and the contact angle θ . (b) We assume the edge of the solidification front propagates along the contact angle θ , allowing us to compute the shape of the ice-drop, characterized by $R(z)$.

after solidification. The price we pay for these simplifications is that the conical top of the drop does not appear for a solid-liquid density ratio that is typical for water, but only for such smaller values. However, the key advantages of such a simple model is that it can be solved in full detail while still revealing the underlying physics of the singularity. More refined versions of this model have been proposed that are indeed able to quantitatively reproduce the experimental results for realistic density ratios.⁹

Following the assumptions of Fig. 3, the model contains three geometric parameters: the base radius of the unfrozen liquid R , the volume of the remaining liquid V , and the contact angle of the liquid with the ice θ . All of these quantities are functions of the height z of the ice layer. For millimetric drops, the liquid will take the shape of a spherical cap; larger drops will be somewhat flattened by gravity. For simplicity, we focus on small drops and use the geometric expression for the volume of a spherical cap

$$\frac{V_{sc}}{R^3} = \frac{\pi}{3} \left(\frac{2 - 3\cos\theta + \cos^3\theta}{\sin^3\theta} \right), \quad (2)$$

which provides a first relation between the three parameters V , R , and θ .

A second relation comes from the assumption that the freezing process is directed along the water–vapor interface, which gives a relationship between the contact angle θ defined for the fluid and the slope of the solid ice, giving (Fig. 3)

$$dR = -\frac{dz}{\tan\theta}. \quad (3)$$

Finally, the evolution of the liquid volume is given by mass conservation: an increase in solid mass (ice) of $\rho_s dV_s$ results in an equal decrease in liquid mass of $-\rho_\ell dV$. Here, we denote ρ_s and ρ_ℓ as the solid and liquid densities, respectively. Using $dV_s = \pi R^2 dz$ then gives

$$dV = -\frac{\rho_s}{\rho_\ell} \pi R^2 dz. \quad (4)$$

Equations (3) and (4) provide two differential equations for the system

$$\frac{dR}{dz} = -\frac{1}{\tan\theta}, \quad (5)$$

$$\frac{dV}{dz} = -\nu\pi R^2, \quad (6)$$

where we have introduced the density ratio $\nu = \rho_s/\rho_\ell$, a parameter that plays a key role in this problem. Once the initial radius and volume are specified, Eqs. (5) and (6), along with the volume constraint (2), completely determine the shape of the drop $R(z)$.

As discussed in Appendix A, differentiating Eq. (2) with respect to z and making use of Eqs. (5) and (6) leads to a system of two coupled equations for R and θ given by

$$\frac{d\theta}{dz} = -\frac{1}{R} [\nu - (1 - \nu)(2\cos\theta + \cos^2\theta)], \quad (7)$$

$$\frac{dR}{dz} = -\frac{1}{\tan\theta}. \quad (8)$$

This system can be solved analytically for $R(\theta)$, although the derivation for arbitrary ν is cumbersome (see Appendix A for details). However, it is instructive to discuss the limiting case $\nu = 1$ for which there is no change in density upon freezing. In this case, Eqs. (7) and (8) can be recast as

$$\frac{dR}{d\theta} = \frac{R}{\tan\theta}, \quad (9)$$

and solved to give

$$R(\theta) = \frac{R_0 \sin\theta}{\sin\theta_0}, \quad (10)$$

where R_0 and θ_0 are the initial radius and contact angle, respectively. Physically, this solution corresponds to a perfect sphere with radius of curvature $R_0/\sin\theta_0$. This is to be expected because when $\nu = 1$ there is no density change during freezing. Therefore, the volume of the spherical cap is conserved, which leads to no change in shape.

B. Numerical results

We generated drop profiles by numerical integration of Eqs. (7) and (8). Because θ and R both appear explicitly in these equations, numerical integration is straightforward using software such as MAPLE, MATHEMATICA, or MATLAB. Our numerical results are shown for two different contact angles in Fig. 4. The two plots show the drop profiles $R(z)$ after freezing on substrates with different initial contact angles, with each curve corresponding to a different values of the density ratio ν . We observe the following trends. First, for $\nu = 1$, the drop retains its original spherical shape, as predicted above. These are shown as thick solid lines in the two figures. (The fact that the spherical solution appears slightly flattened in this figure is due to a difference in the horizontal and vertical scales.) Second, the top of the drop becomes increasingly pointy as the density ratio is decreased below $\nu = 1$. In fact, there appears to be a critical density ratio below which the top of the drop takes the shape of a cone with a well-defined angle. In Sec. IV, we show that conical drops appear at the critical value $\nu_c = 3/4$ (these shapes are depicted with dashed curves in Fig. 4). For $\nu > \nu_c$, the drops still exhibit a rounded top; indeed, in the regime $\nu > 1$, the drops are flattened with respect to their original spherical shape. Although the shapes obtained for $\nu < \nu_c$ are reminiscent of those observed experimentally (Fig. 1), the agreement is not quantitatively accurate in terms of the parameter ν . Namely, for ice and water, the density ratio is close to $\nu = 0.9$, in which case the model predicts drops that are fairly rounded. Nevertheless, the model does provide insight into how such singular structures can arise.

Despite the obvious differences in shape between Figs. 4(a) and 4(b), the properties of the tips appear to be the same for both cases. To investigate this in more detail, we analyze the slope $|dz/dR|$ for all profiles. The simplest way to obtain this slope is to take a finite difference between the last two datapoints as close as possible to $R = 0$; the actual point $R = 0$ cannot be included in the numerical scheme because R appears in the denominator of Eq. (7). For the current data, the closest distance to the tip was of order 10^{-5} . The results are shown in Fig. 5 where the tip angles for hydrophilic drops (circles) and hydrophobic drops (triangles) are superimposed. Indeed, the tip angles agree very well except for

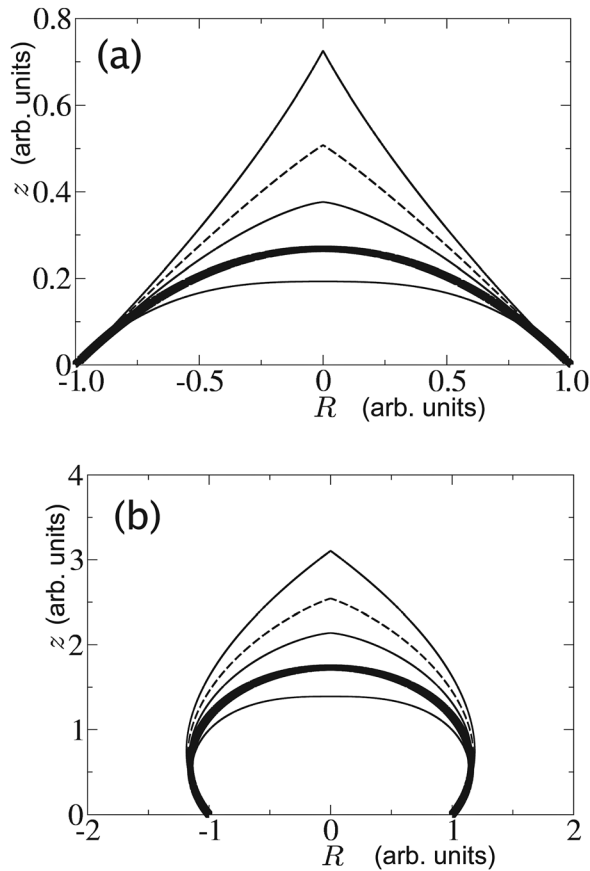


Fig. 4. Numerical solution of the model for ice-drops. (a) Hydrophilic surface with initial contact angle $\theta = 30^\circ$. (b) Hydrophobic surface with initial contact angle $\theta = 133.5^\circ$. The curves correspond to density ratios $\nu = 0.65, 0.75, 0.85, 1, 1.2$ (top to bottom), with initial radius $R_0 = 1$. The thick solid curve represents the original spherical cap ($\nu = 1$), while the dashed curve is the critical case separating “rounded” from “conical” drops ($\nu = 3/4$). Note that the profiles are slightly flattened due to a difference in horizontal and vertical scales.

the case $\nu = 3/4$. From the analysis in Sec. IV, it will become clear that $\nu = 3/4$ marks a critical point for which the numerical resolution requires a higher accuracy than used in the current simulations. In principle, we could

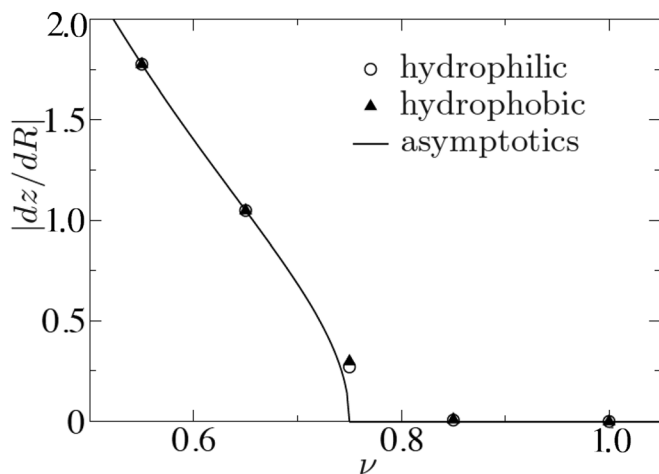


Fig. 5. Numerical determination of the tip angle. The circles and triangles are the slope $|dz/dR|$ near the tip for the profiles in Fig. 4. The tip angle only depends on ν and agrees with the analytical prediction (solid line) derived in Sec. IV.

improve our time-stepping for the case $\nu = 3/4$, but here we intentionally kept the numerical accuracy identical for all values of ν to emphasize the general point that a critical point is difficult to resolve numerically. The fact that the tip structure is independent of large scale details of the drop is a generic feature of singularities called *universality*.¹⁷ This term means that the structure near the singularity is independent of any details far from the singularity—it is “universal.” For the present model, we can indeed show that, for a given value of ν , the shape of the tip is independent of the initial volume or contact angle.

IV. ASYMPTOTIC ANALYSIS OF THE SINGULARITY

It is usually rather difficult to approach a singularity in a numerical simulation. In the example above, one has to increase the numerical resolution to determine the detailed structure of the tip of the ice-drop. Perhaps surprisingly, it turns out that the vicinity of the singularity can often be treated analytically in full detail, even when the problem itself has no exact solution. The mathematical trick is to define a variable that quantifies the “distance” to the singularity. One can then analyze the simplified expressions that result when taking the limit that this distance goes to zero. This method is called asymptotic analysis.

Let us denote the maximum height of the ice drop as z_0 . A natural choice for the distance to the singularity is

$$y = z_0 - z, \quad (11)$$

and we will analyze the drop shape as $y \rightarrow 0$. Given the simulation results, we anticipate two regimes: $\nu < \nu_c$, for which a cone is formed, and $\nu > \nu_c$, which yields rounded drops. The goal of this section is to determine the value of ν_c , the nature of the bifurcation, and the (asymptotic) shapes near the top of the drop for arbitrary values of ν .

A. Conical drops: $\nu < \nu_c$

We assume that the top of the drops has a conical shape with angle ϕ , as shown in Fig. 6. We will show that the value of ϕ depends only on the density ratio ν . The drop profile can be represented as $R = y \tan \phi$. This angle relates to a

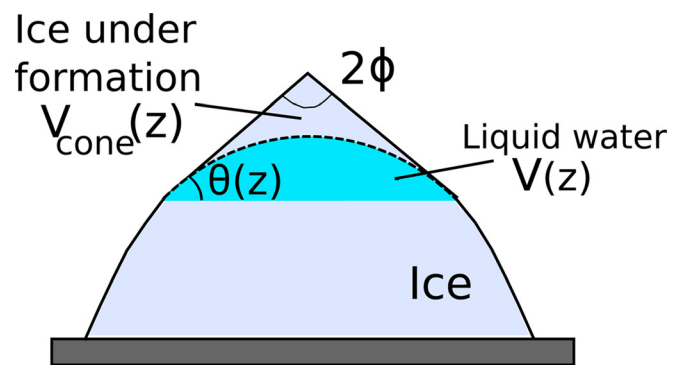


Fig. 6. Physical interpretation of the cone formation. To create a conical tip, the liquid mass stored in the unfrozen spherical cap has to be transformed into the conical ice mass (denoted as “ice under formation”). Since the volume of the (solid) cone is clearly larger than that of the (liquid) spherical cap, the cone can only appear when the solid has a lower density than the liquid. More precisely, one requires $\nu < \nu_c = 3/4$ as discussed in the text.

“base” angle $\theta = \pi/2 - \phi$ that is constant, and thus independent of z along the cone. The model equations (5) and (6) are then easily integrated to give

$$R = \frac{y}{\tan \theta}, \quad (12)$$

$$V = \frac{\nu \pi y^3}{3 \tan^2 \theta}. \quad (13)$$

The latter equation gives the volume of water necessary to fill the ice cone shown in Fig. 6. To see this more clearly, Eq. (13) can be expressed as

$$V = \nu \left(\frac{1}{3} \pi R^2 y \right) = \nu V_{\text{cone}}, \quad (14)$$

which is nothing but the volume of the ice cone multiplied by ν to obtain the equivalent liquid volume. For graphing purposes, it is convenient to write Eq. (13) in dimensionless form as

$$\frac{V}{R^3} = \frac{\nu \pi}{3} \tan \theta. \quad (15)$$

As illustrated in Fig. 6, the mass inside the ice cone has to match that of the unfrozen liquid stored inside the spherical cap. For a given density ratio ν , this condition is only fulfilled for a single angle θ . Mathematically, this angle is obtained by equating the two masses, $\rho_\ell V_{\text{sc}} = \rho_s V_{\text{cone}}$, or equivalently, by equating the volume of the spherical cap to the volume given in Eq. (13) or (14): $V_{\text{sc}} = V$; the top angle of the cone then follows simply as $\phi = \pi/2 - \theta$. This solution procedure is sketched in Fig. 7. The thick solid curve represents the volume of the spherical cap as given by Eq. (2). The other curves are given by Eq. (15), plotted for different values of ν . Clearly, only the thin solid curve displays an intersection corresponding to a cone solution. For values of ν beyond a critical value, there is no intersection and hence no conical solutions exist. To determine this critical value, we look for when the volume curve is tangent to

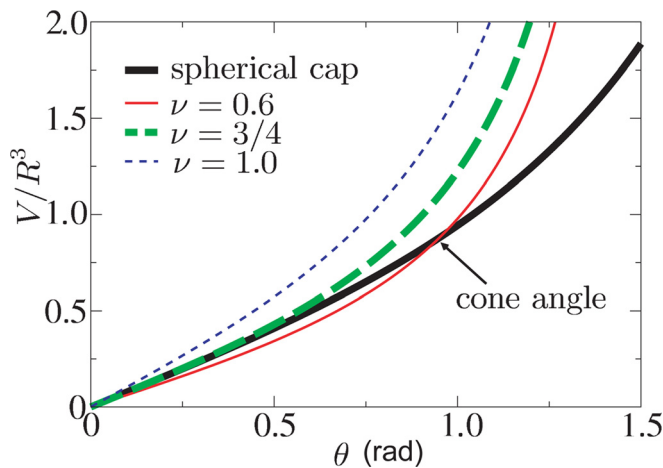


Fig. 7. Geometric relations for the normalized volume V/R^3 . The thick solid curve shows the volume of a spherical cap given by Eq. (2); the other curves show the volumes according to Eq. (15). No intersection with the spherical cap is found for $\nu > 3/4$ (thin dashed), while a finite cone angle can be determined for $\nu < 3/4$ (thin solid). The critical curve corresponds to $\nu_c = 3/4$ (thick dashed).

the spherical cap curve at $\theta = 0$. Mathematically, we equate the slopes of the volume curves (2) and (15) at $\theta = 0$. Carrying out the differentiation, we find that $V'_{\text{sc}}(0) = \pi R^3/4$ and $V'(0) = \nu \pi R^3/3$, which are identical for $\nu_c = 3/4$.

It turns out that this graphical solution can be represented by the simple analytical formula

$$\theta = \arccos\left(\frac{1}{\sqrt{1-\nu}} - 1\right). \quad (16)$$

The interested reader can find the derivation of this result in Appendix A. This relation is plotted as the solid curve in Fig. 8 and forms the basis for the solid curve in Fig 5. In the vicinity of the critical point, we see that $\theta \rightarrow 0$ (or $\phi \rightarrow \pi/2$) as expected. We also see that the cone angle θ increases (or equivalently ϕ decreases) for smaller ν , which is consistent with our numerical findings. Note the typical “square-root” behavior near the critical point, which is characteristic for a supercritical bifurcation. For $\nu > 3/4$, the argument of the arccos function becomes greater than 1, rendering Eq. (16) undefined. To determine the shape of the drops in this regime requires further analysis.

B. Rounded drops: $\nu > \nu_c$

We now turn to the question of what happens when $\nu > \nu_c = 3/4$, when the drops do not exhibit a conical tip. From the numerical solutions, we know that the top is rounded and is thus characterized by a vanishing contact angle $\theta \ll 1$. One can take advantage of this fact by approximating the volume of the spherical cap volume for small angles. Taking $\theta \ll 1$ in Eq. (2) gives

$$\frac{V}{R^3} = \frac{V_{\text{sc}}}{R^3} \simeq \frac{\pi}{4} \theta, \quad \Rightarrow \quad \frac{1}{\tan \theta} \simeq \frac{\pi R^3}{4V}. \quad (17)$$

The model equations (2), (5), and (6) are then substantially simplified by eliminating θ . Again using $y = z_0 - z$, we obtain

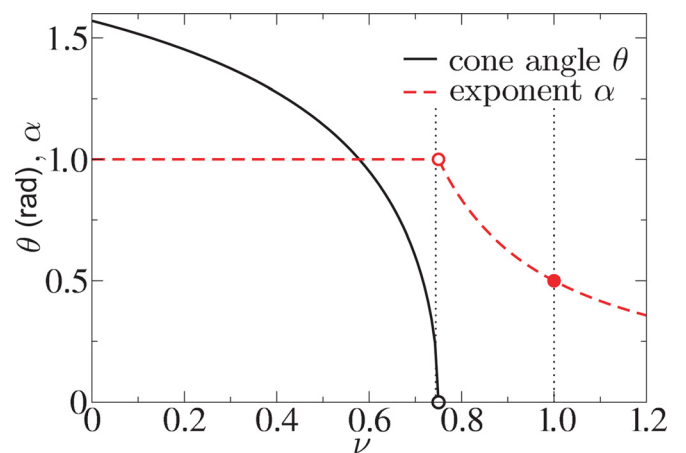


Fig. 8. Bifurcation diagram for different density ratios ν . Base angle of the cone θ for drops with $\nu < 3/4$ (solid curve). The cone angle approaches 0 in the vicinity of the critical point $\nu_c = 3/4$, marking the transition between rounded and conical drops. Exponent α that characterizes the shape of the tip as $R \sim (z_0 - z)^\alpha$ (dashed curve). In the conical regime $\alpha = 1$, while $\alpha < 1$ in the rounded regime. The closed circle represents $\nu = 1$ for which the drop remains spherical ($\alpha = 1/2$). The curve excludes the critical point (open circle) because the shape displays logarithmic corrections to the power law.

$$\frac{dR}{dy} = \frac{\pi R^3}{4V}, \quad (18)$$

$$\frac{dV}{dy} = \nu \pi R^2. \quad (19)$$

We will look for power-law solutions of the form

$$R = Ay^\alpha, \quad V = \pi B y^\beta, \quad (20)$$

but first note that the conical solutions have a linear shape $R \sim y$ ($\alpha = 1, \beta = 3$), while the top of a spherical cap will be approximately quadratic $R^2 \sim y$ ($\alpha = 1/2, \beta = 2$).

The general solution for α and β can be determined by substituting the power-law Ansatz into Eqs. (18) and (19) to get

$$\alpha A y^{\alpha-1} = \frac{A^3}{4B} y^{3\alpha-\beta}, \quad (21)$$

$$\beta B y^{\beta-1} = \nu A^2 y^{2\alpha}. \quad (22)$$

Equating powers of y leads to

$$2\alpha - \beta + 1 = 0, \quad (23)$$

while equating the prefactors, we find

$$4\alpha = \frac{\beta}{\nu}. \quad (24)$$

Combining Eqs. (23) and (24) yields the key result of the analysis, that α and β depend only on the density ratio as

$$\alpha = \frac{1}{4\nu - 2}, \quad \beta = \frac{4\nu}{4\nu - 2}. \quad (25)$$

The dependence of α on ν is shown as the dashed curve in Fig. 8. Note that only solutions with $\alpha < 1$ are consistent with the assumption of $\theta \ll 1$, which in practice means $\nu > 3/4$. For $\nu < 3/4$ one instead observes perfectly conical tips ($\alpha = 1$) as discussed above. The critical solution $\nu_c = 3/4$ will be discussed separately below.

The result of this analysis tells us that all solutions for $\nu > 3/4$ have a rounded top: since $\alpha < 1$, the angle at the top is $\theta = 0$. It is interesting to compute the sharpness of the tip, characterized by the curvature

$$\kappa = \frac{R''}{(1 + R'^2)^{3/2}} \sim y^{1-2\alpha}. \quad (26)$$

We see that the curvature at the tip ($y=0$) diverges for $1/2 < \alpha < 1$, which corresponds to the range $3/4 < \nu < 1$. So despite the fact that these drops are rounded, the tip is infinitely sharp. Conversely, drops with $\nu > 1$ have a zero curvature at $y=0$ and are therefore extremely flat. The separating case $\nu = 1$ corresponds to the spherical cap, identical to the initial liquid drop, with finite curvature.

C. Critical drops: $\nu_c = 3/4$

The critical density ratio $\nu_c = 3/4$ must be considered separately because the solution is neither a cone nor a perfect power-law. From Eq. (25), one may be inclined to

think that the critical case simply gives $\alpha = 1$, corresponding to a conical shape. However, according to Eq. (16), the corresponding cone would be completely opened up with an angle $\phi = \pi/2$. As shown in Appendix A, it is possible to obtain the critical solution in the form $R(\theta)$. In the vicinity of the singularity, this solution can be expanded as

$$\theta \simeq \frac{1}{\sqrt{-\ln R}}, \quad \text{or} \quad R \simeq y\sqrt{-\ln y}, \quad (27)$$

confirming that the shape is indeed not a cone—the angle θ depends weakly (logarithmically) on R . Ultimately, however, one finds that $\theta \rightarrow 0$ so that the drop is rounded. This explains, in hindsight, why the numerical results in Fig. 5 differ from the theoretical curve at the critical point ν_c —the slow, logarithmic convergence towards $\theta = 0$ requires a much greater numerical accuracy in the vicinity of the tip.

V. DISCUSSION: EDGE EFFECTS

We have shown that the freezing of water drops on a cold surface provides a beautiful introduction to the physics of singularities. We discuss experimental, numerical, and analytical methods to study the formation of the sharp tip, all of which are applicable within a classroom environment. Despite various approximations, the model contains the essential physics of the tip formation, namely, the singularity only appears if the liquid expands upon solidification.

To arrive at a more quantitative agreement with experiments, which requires conical tip formation for a density ratio of $\nu \approx 0.9$, would necessitate a more detailed model. For example, it has been shown that a realistic prediction for the appearance of the tip is obtained by assuming a growth angle that is determined by dynamical wetting conditions.⁹ In essence, this means that the freezing no longer occurs perfectly along the liquid–vapor interface, as was assumed in our simplified model. In contrast, a more detailed numerical study that resolves the heat transfer problem in more detail, obtains realistic results by keeping the growth along the interface.¹⁶ In this case, it is found that the freezing front is strongly curved and thus not horizontal. At present, there is no experimental evidence that can discriminate which of these mechanisms is most relevant.

Finally, let us comment that the singular tips are preferential sites for the formation of ice crystals after the freezing of the liquid is complete. Leaving the drops for a few minutes, one observes the deposition of water vapor from the air on the top of the drops in the form of tiny ice crystals. This can already be seen in Figs. 1 and 9(a). We argue that this is another beautiful example of “edge effects,” as described by Bocquet¹⁸ in the context of the baking of potato wedges.

The limiting factor for the formation of ice crystals is the transport of vapor molecules towards the frozen ice-drop. The deposits thus grows fastest at locations where the vapor diffusion is most efficient. One can easily understand why this naturally occurs at the sharp tip. To this end, recall that the diffusive flux \mathbf{J} depends on the gradient of the vapor concentration as

$$\mathbf{J} = -D\nabla c, \quad (28)$$

where $c(x,y,z)$ is the vapor concentration field outside the drop and D is the diffusion constant. In turn, the concentration is

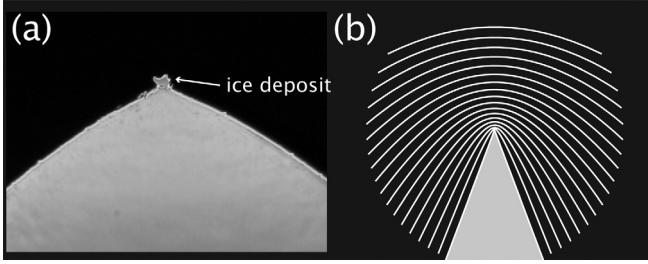


Fig. 9. (a) Photograph of the tip after the drop is completely frozen. The sharp tip is a preferential site for the deposition of the surrounding vapor to form tiny ice crystals. (Image courtesy of Oscar Enriquez, Koen Winkels, and Alvaro G. Marin.) (b) Model calculation for the vapor concentration $c(x, y, z)$ around a perfectly conical tip (see Ref. 18 for details). The white lines are contours of iso-concentration. Clearly, the concentration field develops very large gradients near the singular tip. This is where vapor transport will be most efficient to form ice crystals.

obtained from the steady diffusion equation $\nabla^2 c = 0$ (Laplace's equation). If the concentration at the cone interface is approximately constant, the problem for c is mathematically identical to the electrical potential near a sharp conducting tip. In this analogy, the vapor flux \mathbf{J} behaves as the electrical field, which is known to diverge upon approaching a sharp tip.¹⁸ A typical example for the concentration field (or electric potential) around a sharp tip is shown in Fig. 9(b); the flux is largest where the lines are closest together. Hence, similar to how a lightning rod attracts a flow of charge, the sharp tip of the ice-drop attracts a flow of water vapor that forms tiny crystals.

ACKNOWLEDGMENTS

The authors gratefully acknowledge Alvaro G. Marin, Oscar Enriquez and Koen Winkels for providing the photograph of Fig. 9(a) as well as for discussions on the manuscript.

APPENDIX A: DETAILS ON THE GEOMETRIC MODEL

Here, we briefly discuss the numerical solution of the model, defined by Eqs. (2), (5), and (6). The latter of these equations are coupled differential equations for R and V that require the value of $\tan \theta$. This angle is defined implicitly by Eq. (2), but unfortunately we cannot find a closed-form expression in terms of R and V . One solution strategy would thus be to numerically solve for θ from Eq. (2) for each integration step of Eqs. (5) and (6). Here, we propose another strategy. Differentiating V_{sc} with respect to z gives

$$\frac{dV_{sc}}{dz} = -\frac{1}{\tan \theta} \frac{\partial V_{sc}}{\partial R} + \frac{\partial V_{sc}}{\partial \theta} \frac{d\theta}{dz}, \quad (\text{A1})$$

where we used $dR/dz = -1/\tan \theta$. Equating Eq. (A1) to Eq. (6) allows us to eliminate

$$\frac{d\theta}{dz} = \frac{1}{\partial V_{sc}/\partial \theta} \left(\frac{1}{\tan \theta} \frac{\partial V_{sc}}{\partial R} - \nu \pi R^2 \right). \quad (\text{A2})$$

Working out the partial derivatives then gives the two coupled differential equations

$$\frac{d\theta}{dz} = -\frac{1}{R} [\nu - (1 - \nu)(2 \cos \theta + \cos^2 \theta)], \quad (\text{A3})$$

$$\frac{dR}{dz} = -\frac{1}{\tan \theta}. \quad (\text{A4})$$

The advantage of this approach is that these equations only involve θ and R , both of which appear explicitly. This makes the numerical integration very straightforward.

Equation (A3) also has a number of benefits for analysis. For example, the cone angle can easily be identified because $d\theta/dz = 0$. The corresponding value of θ can be found by making the numerator vanish

$$\nu - (1 - \nu)(2 \cos \theta + \cos^2 \theta) = 0. \quad (\text{A5})$$

This is a simple quadratic equation for $\cos \theta$, whose solution

$$\cos \theta = \frac{1}{\sqrt{1 - \nu}} - 1 \quad (\text{A6})$$

is given in Eq. (16). An even more interesting observation is that one can combine Eqs. (A3) and (A4) to get the separable equation

$$\frac{dR}{R} = \frac{d\theta}{\tan \theta [\nu - (1 - \nu)(2 \cos \theta + \cos^2 \theta)]}. \quad (\text{A7})$$

Indeed, both terms can be integrated, although the expression for general ν is rather elaborate and not particularly enlightening. We therefore present only two interesting cases. First, for $\nu = 1$, one obtains

$$\ln\left(\frac{R}{R_0}\right) = \ln\left(\frac{\sin \theta}{\sin \theta_0}\right), \Rightarrow R = \frac{R_0 \sin \theta}{\sin \theta_0}, \quad (\text{A8})$$

where θ_0 is the initial contact angle. As discussed in Sec. III A, this is the formula for a spherical cap with radius of curvature $R_0/\sin \theta_0$, demonstrating that for $\nu = 1$ the original spherical shape is preserved. Second, the critical solution $\nu = 3/4$ gives

$$\ln\left(\frac{R}{K}\right) = \frac{1}{2(\cos \theta - 1)} - \frac{3}{8} \ln(3 + \cos \theta) - \frac{1}{8} \ln(1 - \cos \theta) + \frac{1}{2} \ln(1 + \cos \theta), \quad (\text{A9})$$

where K is a constant of integration that depends on the initial conditions. We are mainly interested in the structure of the singularity, which is obtained by expanding for small θ , yielding

$$\theta(R) = \frac{1}{\sqrt{-\ln(R/K)}}. \quad (\text{A10})$$

This reveals a logarithmic dependence of the angle on R . Ultimately, this drop is rounded since $\theta(0) = 0$.

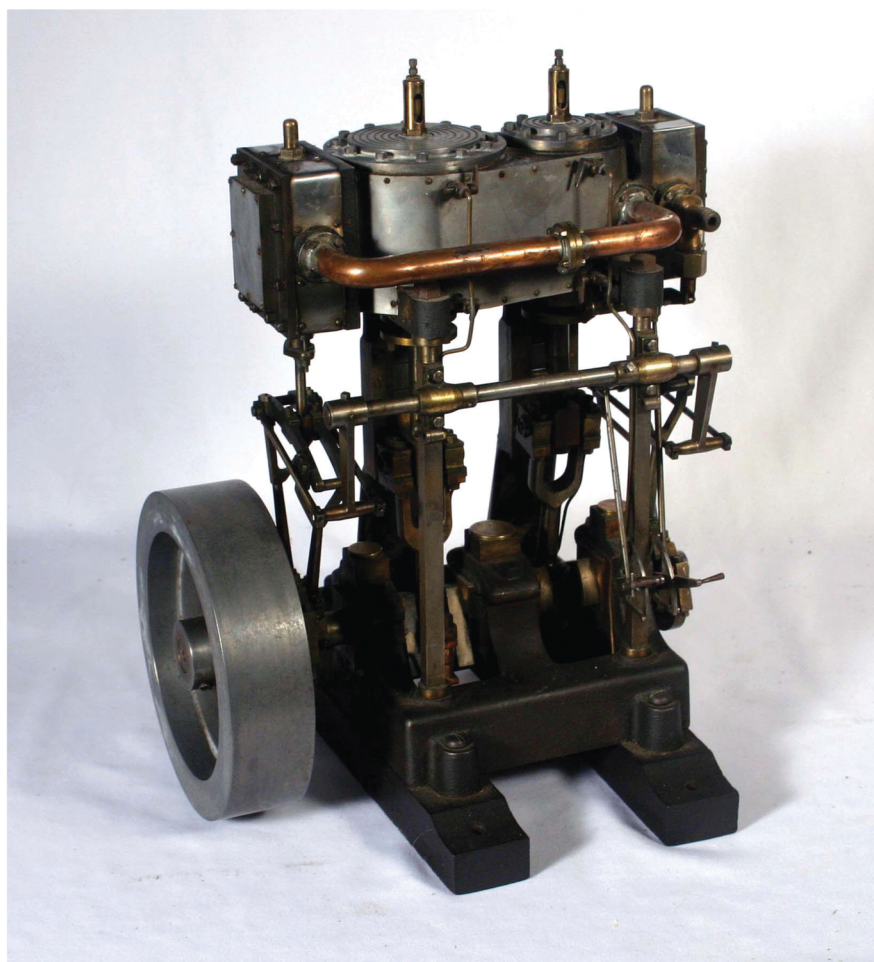
¹J. Eggers, "Universal pinching of 3D axisymmetric free-surface flow," *Phys. Rev. Lett.* **71**, 3458–3460 (1993).

²T. D. Blake and K. J. Ruschak, "Maximum speed of wetting," *Nature (London)* **282**, 489–491 (1979).

³T. Podgorski, J.-M. Flesselles, and L. Limat, "Corners, Cusps, and Pearls in Running Drops," *Phys. Rev. Lett.* **87**, 036102 (2001).

⁴I. Cohen and S. R. Nagel, "Scaling at the selective withdrawal transition through a tube suspended above the fluid surface," *Phys. Rev. Lett.* **88**, 074501 (2002).

- ⁵S. Courrech du Pont and J. Eggers, "Sink flow deforms the interface between a viscous liquid and air into a tip singularity," *Phys. Rev. Lett.* **96**, 034501 (2006).
- ⁶J. Fernandez de la Mora, "The fluid dynamics of Taylor cones," *Annu. Rev. Fluid. Mech.* **39**, 217–243 (2007).
- ⁷I. Peters, J. H. Snoeijer, A. Daerr, and L. Limat, "Coexistence of two singularities in dewetting flows: Regularizing the corner tip," *Phys. Rev. Lett.* **103**, 114501 (2010).
- ⁸E. Lorenceau, F. Restagno, and D. Quéré, "Fracture of a viscous liquid," *Phys. Rev. Lett.* **90**, 184501 (2003).
- ⁹D. M. Anderson, M. Grae Worster, and S. H. Davis, "The case for a dynamic contact angle in containerless solidification," *J. Cryst. Growth* **163**, 329–338 (1996).
- ¹⁰A. Sanz, J. Meseguer, and L. Mayo, "The influence of gravity on the solidification of a drop," *J. Crystal Growth* **82**, 81–88 (1987).
- ¹¹See, for example, SKYbrary, "In-flight icing," <http://www.skybrary.aero/index.php/In-Flight_Icing>.
- ¹²Z. Liu, Y. Gou, J. Wang, and S. Cheng, "Frost formation on a super-hydrophobic surface under natural convection conditions," *J. Heat Mass Transfer* **51**, 5975–5982 (2008).
- ¹³M. He, J. Wang, H. Li, X. Jin, J. Wang, B. Liu, and Y. Song, "Super-hydrophobic film retards frost formation," *Soft Matter* **6**, 2396–2399 (2010).
- ¹⁴K. W. Kolasinski, "Solid structure formation during the liquid/solid phase transition," *Curr. Opin. Solid State Mater. Sci.* **11**, 76–85 (2007).
- ¹⁵D. Bonn, J. Eggers, J. Indekeu, J. Meunier, and E. Rolley, "Wetting and spreading," *Rev. Mod. Phys.* **81**, 739–805 (2009).
- ¹⁶V. S. Ajaev and S. H. Davis, "Boundary-integral simulations of containerless solidification," *J. Comp. Phys.* **187**, 492–503 (2003).
- ¹⁷J. Eggers and M. A. Fontelos, "The role of self-similarity in singularities of PDE's," *Nonlinearity* **22**, R1–R44 (2009).
- ¹⁸L. Bocquet, "Tasting edge effects," *Am. J. Phys.* **75**, 148–150 (2007).
- ¹⁹O. R. Enriquez, A. G. Marin, K. G. Winkels, and J. H. Snoeijer, "Freezing singularities in water drops," arXiv:1110.3698.



Model of Marine Double-Expansion Steam Engine

By the middle of the 19th century, it was realized that it was uneconomical to exhaust into the atmosphere the relatively high-pressure steam from existing single cylinder steam engines. A second cylinder with a larger cylinder diameter was added to use this exhaust steam, thus forming a double expansion engine. Later the design was expanded to include a third cylinder, and this represented the high point of marine steam engine design. In the early years of the 20th century the Parsons steam turbine replaced the reciprocating steam engine in warships and liners, leaving the older and cheaper designs in use until the advent of the large-scale diesel engine. This model of a double expansion engine is about 25 cm high and is in the Greenslade Collection. Note that the cylinder region at the top has heavy thermal insulation. (Notes and photograph by Thomas B. Greenslade, Jr., Kenyon College)